Petroleum Science 22 (2025) 5166–5175

Contents lists available at ScienceDirect

Petroleum Science

journal homepage: www.keaipublishing.com/en/journals/petroleum-science

Original Paper

Imbibition mechanism analysis of modified black nanosheet and low salinity water composite system for enhanced oil recovery by NMR method

Si Guo, Jiong Zhang, Ying-Qi Gao, Hong-Gen Tan, Hong-Bin Cheng, Hong-Yu Li, Dao-Yi Zhu *

China University of Petroleum-Beijing at Karamay, Karamay, 834000, Xinjiang, China

ARTICLE INFO

Article history:
Received 10 June 2025
Received in revised form
17 August 2025
Accepted 18 August 2025
Available online 22 August 2025

Edited by Yan-Hua Sun

Keywords:
Black nanosheets
Low salinity water
Composite imbibition system
Low-permeability reservoir
Imbibition mechanism

ABSTRACT

Black nanosheets (BN, with a specific chemical composition of molybdenum disulfide) have been widely studied for low-permeability reservoir development due to their unique nanoscale dimensions and lamellar structure. Our prior research demonstrated that cationically modified BN combined with low-salinity water (LSW) significantly enhances oil displacement. This study compared the imbibition adaptability of the composite system under both ambient-pressure and pressurized conditions, while combining nuclear magnetic resonance (NMR) techniques to analyze related imbibition mechanisms and reservoir permeability adaptability. Results showed that the modified BN-LSW composited system achieved an imbibition recovery efficiency of 43.92% under ambient pressure. The mechanism was capillary force-dominated, preferentially displacing oil from small pores by improving core wettability and emulsification. Under pressurized conditions, the driving force became dominant, further increasing recovery efficiency to 56.52%, with the system displacing oil from both large and small pores. Additionally, the system showed optimal adaptability in cores with 0.05×10^{-3} μm^2 permeability. Imbibition efficiency declined at higher/lower permeabilities due to weakened capillary forces or nanoparticle aggregation-induced clogging. This study confirmed that the modified BN-LSW composite system enhanced imbibition stability and recovery efficiency, and combined with nuclear magnetic resonance (NMR) technology, its mechanism was revealed at the microscale. This provided theoretical and technical support for the efficient development of low-permeability reservoirs, with significant engineering value.

1. Introduction

As global energy demand keeps rising, low-permeability reservoirs—key unconventional oil and gas resources—have become a major focus for the petroleum industry (Kang et al., 2022). Conventional water flooding often achieves recovery efficiencies below 30% due to low permeability, complex pore-throat structures, and high capillary resistance (Du, 2023; Yang H.B. et al., 2025). Recently, nanofluid flooding has offered a new approach for low-permeability reservoirs by regulating interfacial properties (Eltoum et al., 2021; Wu et al., 2024a, 2024b). Nanoparticles can improve microscopic displacement efficiency by reducing oil–water interfacial tension (IFT), altering rock wettability, and enhancing emulsification (Liang et al., 2023; Wu et al., 2025; Xu et al., 2023). Among these, black nanosheets (BN, molybdenum disulfide nanomaterials) show strong potential due to their high surface area and adsorption capacity (Feng et al., 2022; Qu et al., 2021; Raj et al., 2019; Xu et al., 2019). However, traditional BN tend to aggregate and destabilize during long-term flooding because of salinity sensitivity, leading to rapid efficiency decline (Xiao and Hou, 2023). Improving their dispersion stability and reservoir adaptability remains a critical challenge for industrial use.

* Corresponding author.
E-mail address: chutaoi@163.com (D.-Y. Zhu).
Peer review under the responsibility of China University of Petroleum (Beijing).

https://doi.org/10.1016/j.petsci.2025.08.026

The BN-LSW composite system (BN + low salinity water) achieves synergistic "1 + 1 > 2" effects (Zhu et al., 2023). LSW (< 5000 mg/L) inhibits clay swelling and reduces ionic strength (Yang et al., 2020), while black nanosheets form rigid interfacial films to enhance crude oil emulsification (Arab et al., 2018; Binks and Whitby, 2005; Zhu et al., 2023). Yet, traditional black nanosheets face two key issues in low-salinity environments: poor dispersion stability due to pH-dependent surface charge fluctuations (Zhu et al., 2024b) and limited permeability adaptability—viscous fingering in high-permeability zones and insufficient capillary-driven displacement in low-permeability zones (Zhu et al., 2025). To address these, surface modification (e.g., silane coupling agents, polymer coatings) has been explored. Qu et al. (2022) developed amphiphilic molybdenum disulfide nanosheets that shift oil-wet surfaces to neutral-wet and generate micro-scale emulsions, improving oil recovery. Zhu et al. (2024b) created a cationic-modified BN using CTAB surfactant, which showed better suspension stability, wettability alteration, and a 12.51-percentage-point increase in core sample recovery. Zhu et al. (2024a) also synthesized an anionic-modified BN with strong charge repulsion and excellent imbibition in ultra-low-permeability cores. However, systematic studies of modification effects and displacement mechanisms are still lacking. Most experiments are conducted at ambient pressure, leaving gaps in understanding high-pressure behavior—a limitation for high-pressure, low-permeability reservoirs (Shao et al., 2023; Xiao et al., 2022).

Research on nanofluid flooding began in the early 21st century, initially using iron oxide nanoparticles to improve heavy oil mobility (Pereira et al., 2020). In recent years, SiO_2, TiO_2, and carbon-based nanomaterials have gained attention due to their low cost and high stability (Manshad et al., 2022; Tang et al., 2022). For example, Liu et al. (2023) developed modified silver nanoparticles by grafting microbial surfactants, achieving a recovery efficiency increase of 11.40%–19.49%. Many studies also focus on optimizing nanoparticle-chemical flooding hybrid systems (Al-Asadi et al., 2022). Paryoto et al. (2023) designed a composite system of Fe_3O_4 nanoparticles and surfactants, with core tests showing a final recovery degree improvement of up to 76.5%. Moradi et al. (2015) introduced silica nanoparticles into water-alternating-gas (WAG) EOR processes, enhancing recovery efficiency. Kang et al. (2021) applied silica nanoparticles in CO_2 foam flooding, improving foam stability, plugging ability, and oil displacement. However, current technologies often require high nanoparticle injection concentrations (> 0.1 wt%) and suffer from poor long-term stability, highlighting the need for low-dose, high-efficiency systems.

Mechanistically, researchers agree that nanofluid flooding efficiency depends on capillary forces, driving forces, and wettability alteration (Zhu et al., 2025; Yang C. et al., 2025; Liu et al., 2019). Zhu et al. (2024a, 2024b) used interfacial tensiometry to measure the IFT between modified black nanosheets and crude oil, finding that while IFT reduction was limited, the nanosheets exhibited strong emulsification and wettability alteration. However, the mechanism shift under pressurized conditions remains unclear. Additionally, the impact of reservoir heterogeneity on nanofluid flooding is debated (Wang et al., 2022). For example, Zhu et al. (2025) observed that permeability below 0.1×10^{-3} μm^2 led to pore-throat clogging and efficiency decline, while others reported effective displacement even at 0.05×10^{-3} μm^2. These contradictions highlight the need for systematic studies on reservoir adaptability.

Therefore, based on previous research on the modified BN-LSW composited system and its displacement performance and ambient-pressure imbibition understanding in low-permeability reservoirs (Zhu et al., 2025), this study compared the imbibition adaptability of the composite system under both ambient-pressure and pressurized conditions, while analyzing related imbibition mechanisms and reservoir permeability adaptability. Imbibition experiments were performed at 0.1 MPa (ambient-pressure) and 5 MPa (pressurized). NMR relaxation spectra quantitatively characterized how the BN-LSW system extracts crude oil from different core pores under varying pressures, revealing the competition between capillary forces and driving forces. Cores with permeabilities from 0.01×10^{-3} to 0.5×10^{-3} μm^2 were tested. The work systematically explored how imbibition efficiency relates to permeability in the modified BN-LSW system, providing theoretical guidance for optimizing nanocomposite technologies in low-permeability reservoir development.

2. Experimental materials and methods

2.1. Experimental materials

The black nanosheet (BN), urea (AR, 99.5%), and cetyltrimethylammonium bromide (CTAB, AR, 99.5%) were all provided by Shanghai Macklin Biochemical Technology Co., Ltd. The black nanosheet consisted of cetyltrimethylammonium bromide (CTAB) and urea-modified molybdenum disulfide (MoS_2), exhibiting a flake-like morphology with an approximate particle size of 70 nm × 400 nm. The sheet thickness was as low as ~10 nm. The formation water had a salinity of 20,512 mg/L, and the crude oil had a viscosity of 7.5 mPa·s, both provided by Xinjiang Oilfield. The formation water was diluted 40 times to serve as the LSW solution for the composite system (Zhu et al., 2025). The ionic composition of the formation water is shown in Table 1, with its water type being $CaCl_2$-type.

2.2. Preparation method of modified black nanosheets

The preparation method of modified BN powder was published by Zhu et al. (2024b). A certain mass of BN powder was uniformly dispersed in 100 mL of deionized water and sonicated for 30 min in an ultrasonic cleaner. A specific mass of CTAB powder and urea was dissolved in the BN dispersion. The mixture was then subjected to condensation reflux at 60 °C, followed by centrifugation at 2500 r/min for 10 min. After centrifugation, the product was suction-filtered and washed three times with deionized water. Subsequently, it was placed in a vacuum freeze dryer for vacuum drying for one week.

2.3. Characteristic method of modified black nanosheets

(1) TEM testing. An appropriate quantity of modified nano-black card (BN) solid powder was dispersed in aqueous so-

Table 1
Salinity and ionic composition of formation water.

Total salinity, mg·L^{-1}	Ion concentration, mg·L^{-1}					
	Na^+	K^+	Ca^{2+}	SO_4^{2-}	Cl^-	HCO_3^-
20512	4826	536	2377	49	12032	690

lution. Morphological characterization was performed using field emission transmission electron microscopy (FEI-Tecnai G2 F20, FEI Company, USA).

(2) Zeta potential measurement. Unmodified and modified BN solutions (0.002 wt%) were prepared, followed by 30-min ultrasonic dispersion. Zeta potential values were measured at 34 °C (93.2 °F) using a zeta potential analyzer (Zetasizer Nano ZS, Malvern Instruments Ltd., UK).

(3) Dispersion stability testing. The modified BN-low salinity water (LSW) composite system underwent 30-min ultrasonic dispersion. Stability was evaluated at 34 °C using a multiple light scattering analyzer (TURBISCAN Lab Expert, Formulaction, France).

(4) Contact angle measurement. Unmodified and modified BN-LSW composite systems were prepared with 30-min ultrasonic dispersion. The three-phase (rock/crude oil/water) contact angles were measured at 34 °C using a goniometer (DSA25, KRÜSS GmbH, Germany) (Zhu et al., 2024b).

2.4. Imbibition experiment under ambient pressure

The core samples were dried in an oven at 105 °C until their weights stabilized. After cooling, the cores were weighed. The oil-saturation experiment was conducted after vacuuming the cores. Following oil saturation, T_2 spectrum tests for fluid distribution analysis were performed, and the cores were weighed again. The oil-saturated cores were then placed in prepared solutions for imbibition experiments. During the experiments, the cores and solutions were maintained in an oven at 34 °C. The core weights were recorded at different time intervals to calculate the oil recovery during spontaneous imbibition. Specifically, the mass of the core after different imbibition times was measured. Based on the mass difference between the core in its initial oil-saturated state and at each imbibition time, combined with the oil-water density difference, the volume of recovered oil was calculated. Finally, the oil recovery factor was determined as the ratio of the recovered oil volume to the original oil volume in the core. The parameters of cores used in imbibition experiments under ambient pressure are shown in Table 2.

2.5. Imbibition experiment under pressurized conditions

Two core samples with the same permeability were dried in an oven at 105 °C. After cooling, their weights were measured until no further mass change was observed. The cores were then vacuumed and saturated with oil. After oil saturation, their masses were recorded. Next, the oil-saturated cores were placed separately into intermediate containers filled with the modified BN-LSW composite system and the unmodified BN-LSW composite system. The intermediate containers were pressurized to 20 MPa. At different time intervals, the cores were removed for mass measurement. They were then placed back into the containers and repressurized to 20 MPa. This aging cycle was repeated until the experiment concluded. The core weights were recorded at different time intervals to calculate the oil recovery during spontaneous imbibition. The parameters of the core samples used in the imbibition experiments under pressurized condition are listed in Table 3.

2.6. NMR T_2 spectrum measurement

A core NMR analyzer (SPEC-RC035, Beijing SPEC Co.) was used to measure the prepared core samples with preset parameters. The T_2 spectrum curves and related data were recorded at different stages including water saturation, oil saturation, during imbibition, and after imbibition. The specific test parameters were set as follows: pulse interval (TAU) 100 μs, sampling interval (DW) 4 μs, scan count (SCAN) 32, and signal gain (RG) 5 dB.

3. Results and discussion

3.1. Basic properties of modified black nanosheet

Fig. 1 presents the fundamental properties of the cationically modified nano-black card (BN). TEM analysis shows that the synthesized modified BN consists of black flaky powder particles with dimensions of 70 nm × 400 nm, demonstrating potential for enhanced oil recovery in low-permeability reservoirs, as illustrated in Fig. 1(a). When prepared under the conditions of 0.2 g BN, 1.2 g urea, 0.8 g CTAB, and a reaction temperature of 60 °C, the modified BN exhibited significantly improved stability compared to unmodified BN.

The modified BN in low-salinity water (LSW) displayed a zeta potential absolute value of 25.9 mV, representing a substantial increase over the unmodified BN-LSW composite system (15.2 mV), which demonstrated that the cationic modification strengthened interparticle electrostatic repulsion among black nanosheets, confirming enhanced dispersion stability (Fig. 1(b)). This conclusion was further supported by macroscopic analysis using a multiple light scattering analyzer, which recorded a Turbiscan stability index (TSI) of just 0.46, indicating markedly improved dispersion stability in aqueous solution compared to unmodified BN, as shown in Fig. 1(c).

Additionally, the contact angle between the modified BN aqueous dispersion and crude oil/rock measured 57.70°, a reduction of 18.40° compared to the unmodified system, as shown in Fig. 1(d) and (e). The modified BN-LSW composite system further decreases the contact angle with crude oil and rock, improving the wettability of oil droplets on rock surfaces. These fundamental property analyses provide critical insights for investigating the subsequent imbibition mechanisms of the BN-LSW composite system.

Table 2
Parameters of the core in imbibition experiments under ambient pressure.

Core No.	Length, cm	Diameter, cm	Gas permeability, 10^{-3} μm^2	Experimental conditions
S1-1	7.03	2.51	1.5	Modified BN-LSW composite system
S1-2	6.98	2.52	1.5	Unmodified BN-LSW composite system
S2-1	7.01	2.49	0.01	Different core permeabilities
S2-2	6.96	2.54	0.05	
S2-3	6.96	2.49	0.5	
S2-4	7.01	2.48	1	
S2-5	7.00	2.49	5	
S2-6	7.01	2.50	50	

Table 3
Parameters of the core in imbibition experiments under pressurized condition.

Core No.	Length, cm	Diameter, cm	Gas permeability, 10^{-3} μm^2	Experimental conditions
C3-1	6.99	2.50	1.5	Modified BN-LSW composite system
C3-2	7.02	2.51	1.5	Unmodified BN-LSW composite system

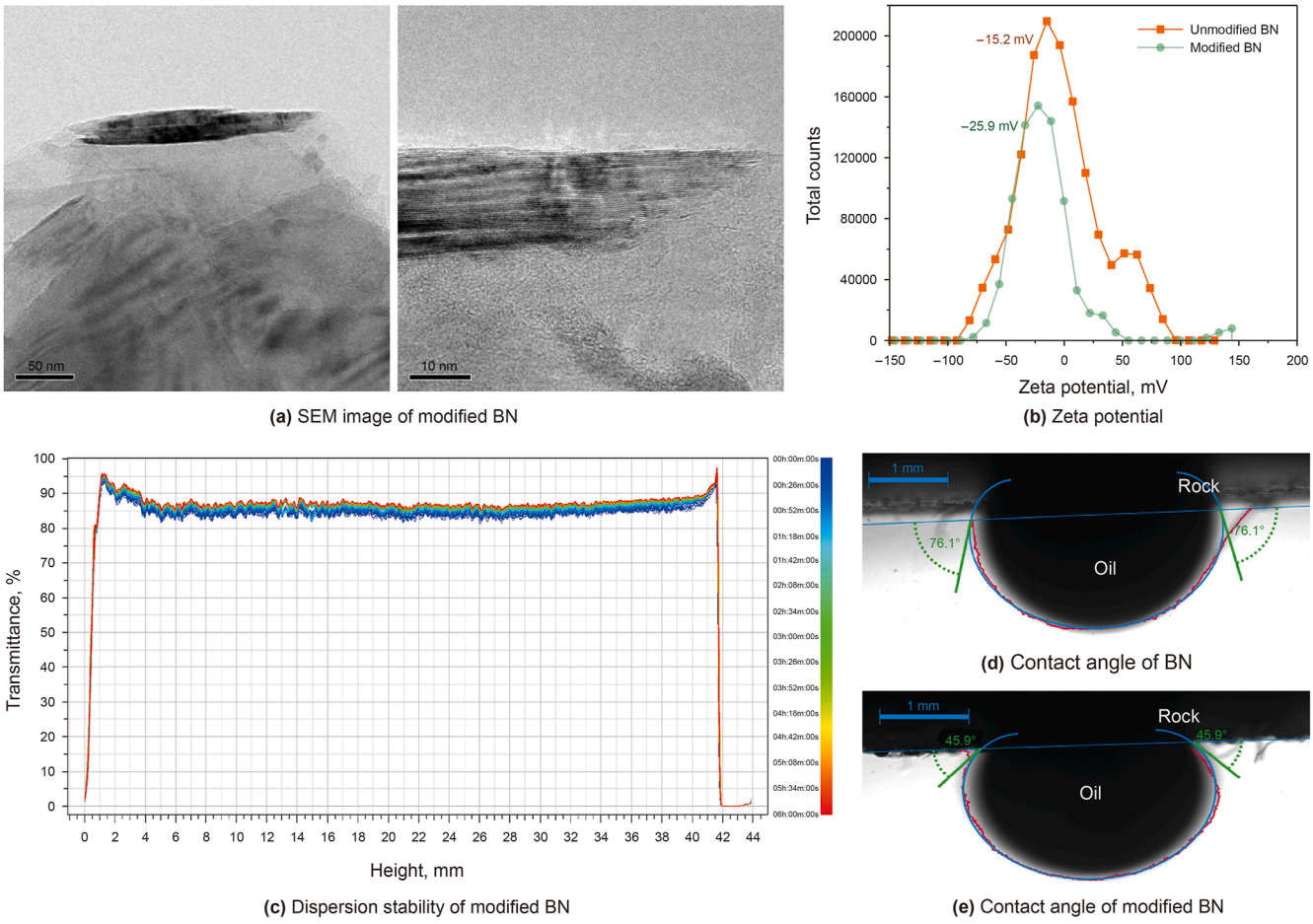

Fig. 1. Fundamental properties of modified black nanosheets.

3.2. Imbibition performance of BN-LSW composite system under ambient pressure

3.2.1. Imbibition recovery of BN-LSW composite system under ambient pressure

The imbibition effects of 0.002 wt% modified BN-LSW composite system and an unmodified BN-LSW composite system on core samples under ambient pressure were investigated through imbibition experiments under ambient pressure (i.e., 0.1 MPa). The dynamic recovery efficiency obtained by the mass measurement method over time was plotted, as shown in Fig. 2.

As shown in Fig. 2, under ambient-pressure imbibition conditions, the crude oil recovery efficiency of oil-saturated core samples in different imbibition systems exhibited a clear increasing trend over time. In the early stage of imbibition, the recovery efficiency increased rapidly and then gradually leveled off. At the end of the imbibition experiment, the final recovery efficiency of the modified BN-LSW composite system reached 43.92%, while that of the unmodified BN-LSW composite system was 39.66%. This indicates that the modified BN-LSW composite system has better imbibition and oil displacement effects under ambient pressure. In addition, the imbibition recovery degree (34.00% OOIP) achieved by formation water at ambient pressure demonstrated that the BN-LSW composite system (both pre-modification and post-modification) exhibited significantly superior imbibition performance compared to formation water.

3.2.2. NMR characteristics analysis of BN-LSW composite system during imbibition under ambient pressure

The imbibition effects of BN-LSW composite system before and after modification on core samples under ambient pressure were analyzed using NMR T_2 spectra. The NMR analysis method was employed to scan fluid saturation in core samples at different time intervals, obtaining the NMR T_2 spectra as shown in Figs. 3 and 4.

From Fig. 3, it can be observed that the T_2 spectrum of the core sample treated with modified BN solution exhibited a bimodal characteristic where the two peaks were demarcated by a relaxation time of 10 ms. Based on mercury injection capillary pressure (MICP) measurements of the core, a relaxation time of 10 ms corresponds to a pore throat diameter of 60 nm. The signal

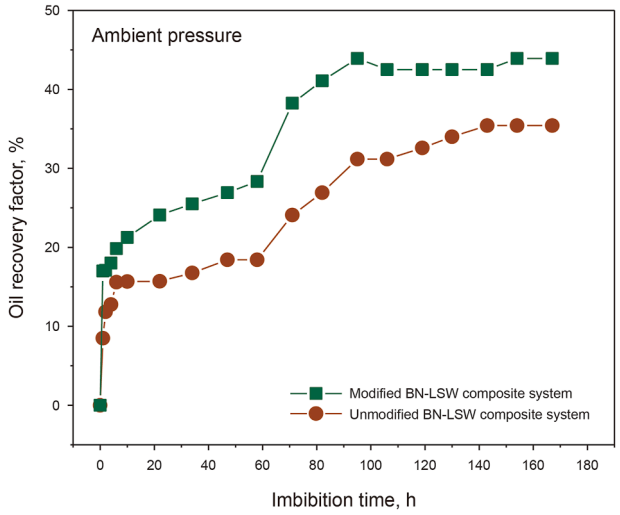

Fig. 2. Oil recovery factor during spontaneous imbibition under ambient pressure for two composite systems.

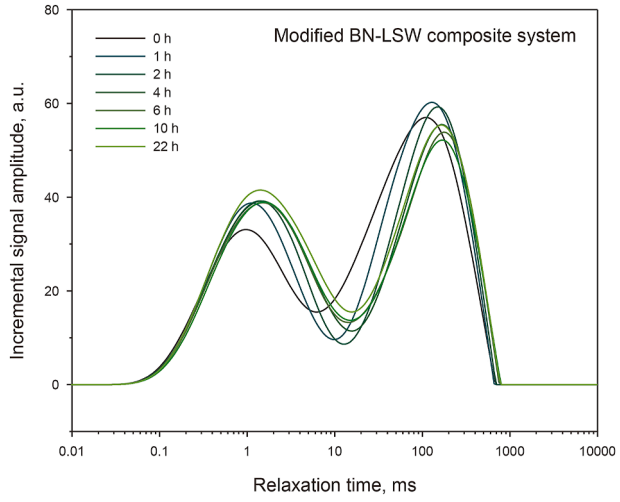

Fig. 3. T_2 spectrum evolution during ambient-pressure imbibition in modified BN-LSW composite system.

amplitude in the small pore region (left peak) continuously increased over time, while the signal amplitude in the large pore region (right peak) first rose, then declined, and then rose again. This indicated that as the imbibition experiment progressed, the modified BN solution continuously entered the small pores of the core under capillary force. The imbibition volume in small pores was large, and the hydrogen protons in the solution continuously filled these pores, leading to a monotonic increase in signal amplitude in the small pore region. In the early stage, the signal amplitude in the large pores of the core increased due to the invasion of the modified BN solution. As imbibition proceeded, the extensive release of crude oil caused the signal to weaken. In the later stage, further saturation of the solution increased the hydrogen proton density, resulting in a renewed enhancement of the signal amplitude.

From Fig. 4, it can be observed that the core sample treated with unmodified BN-LSW solution also exhibits a bimodal T_2 spectrum where the two peaks were demarcated by a relaxation time of 10 ms. Based on MICP measurements of the core, a relaxation time of 10 ms corresponds to a pore throat diameter of 60 nm. The signal

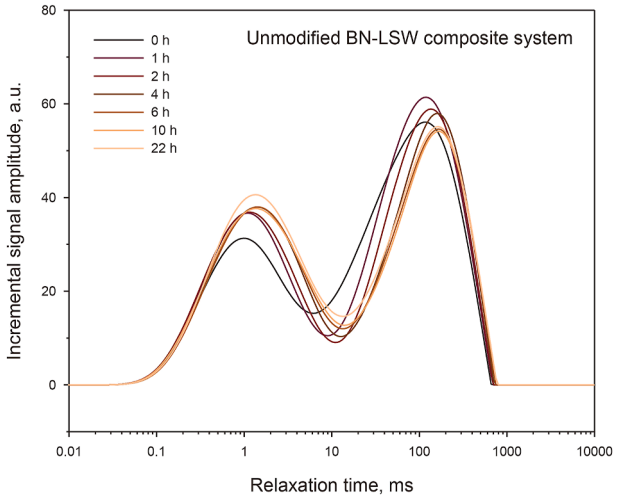

Fig. 4. T_2 spectrum evolution during ambient-pressure imbibition in unmodified BN-LSW composite system.

amplitude in the small pore region (left peak) shows continuous increase over time, while the signal amplitude in the large pore region (right peak) demonstrates an initial increase followed by a decreasing trend. This indicates that during imbibition, the continuous penetration of unmodified BN-LSW solution into small pores leads to a progressive increase in hydrogen proton density. In contrast, the large pore region shows signal amplitude attenuation due to insufficient solution replenishment after crude oil displacement. Overall, the core sample treated with modified BN-LSW solution exhibits more significant curve amplitude variations, suggesting superior imbibition performance compared to the unmodified BN-LSW solution.

To quantitatively evaluate the imbibition performance difference between modified and unmodified BN-LSW solutions under ambient pressure conditions, the variations in T_2 spectrum peak areas of core samples treated with both solutions at different time points were plotted, as shown in Fig. 5.

From Fig. 5, it can be seen that the peak area of the core sample shows continuous growth with prolonged imbibition time. After 6 h of imbibition, the small pore peak area increased by 58.98 a.u. (modified) and 47.47 a.u. (unmodified), while the large pore peak area increased by 2650.20 a.u. (modified) and 2145.10 a.u. (unmodified). This indicates that modified BN-LSW composite system demonstrates excellent oil displacement performance during early imbibition, effectively displacing crude oil in both small and large pores. After 22 h of imbibition, the small pore peak area increased by 87.33 a.u. (modified) and 65.75 a.u. (unmodified), while the large pore peak area increased by 3356.40 a.u. (modified) and 2841.40 a.u. (unmodified). The core sample treated with modified BN-LSW composite system shows greater peak area variation, confirming that the modified BN-LSW composite system has superior imbibition and oil displacement effects.

3.2.3. Imbibition mechanism of modified BN-LSW composite system under ambient pressure

The imbibition mechanism of the modified BN-LSW composite system under ambient pressure was analyzed using imbibition under ambient pressure experiments combined with NMR T_2 spectrum measurements. Fig. 6 illustrates the imbibition mechanism under ambient pressure of oil-saturated core samples under the influence of the modified BN-LSW composite system.

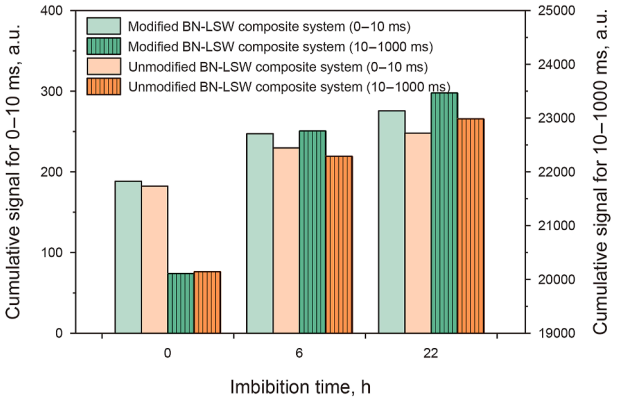

Fig. 5. T_2 peak area evolution during ambient-pressure imbibition in the modified and unmodified BN-LSW composite systems.

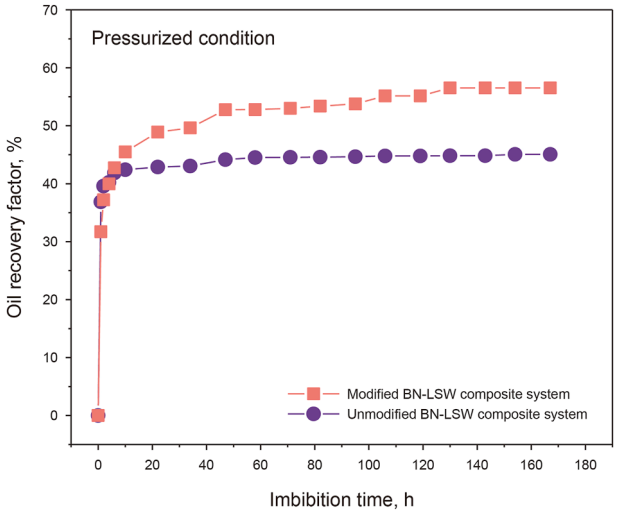

Fig. 7. Comparison of oil recovery after imbibition in different systems under pressurized condition.

From Fig. 6, it can be observed that during imbibition under ambient pressure, the modified BN-LSW solution preferentially enters the small pores of the oil-saturated core sample under capillary force. The modified BN-LSW significantly improves rock wettability, changing the rock surface from hydrophobic to hydrophilic. This effectively removes the oil film on the surface. At the same time, the modified BN-LSW emulsifies with crude oil, significantly reducing oil viscosity and enhancing mobility. This achieves efficient imbibition of oil in small pores. Due to capillary effect, some modified BN-LSW solution enters large pores during early imbibition. As imbibition continues, oil in large pores is gradually displaced.

3.3. Imbibition performance of BN-LSW composite system under pressurized condition

3.3.1. Imbibition performance of BN-LSW composite systems under pressurized condition

Imbibition experiments under pressurized condition were conducted to evaluate the performance of modified and unmodified BN-LSW composite systems. Core samples were placed in 0.002 wt% modified BN-LSW and unmodified BN-LSW solutions for imbibition under pressurized condition. The mass change of core samples was recorded in real-time during imbibition. Oil recovery efficiency at different time points was calculated, and the recovery efficiency vs. time curve was plotted, as shown in Fig. 7.

From Fig. 7, it can be observed that under pressurized conditions, the oil recovery efficiency of oil-saturated core samples in different imbibition systems shows an initial rapid increase followed by gradual stabilization. In the early stage of imbibition, both systems exhibit a high growth trend in recovery efficiency, followed by minor fluctuations. This indicates that, during initial imbibition, pressurization effectively promotes the penetration of the composite system solution into the core, displacing a significant amount of crude oil. At the end of the imbibition experiment under pressurized condition, the oil recovery efficiency in the modified BN-LSW composite system reached 56.52%, while that in the unmodified BN-LSW composite system was 45.05%. This demonstrates that the modified BN-LSW composite system achieves better imbibition performance under pressurized condition.

3.3.2. NMR characteristics of BN-LSW composite systems during imbibition under pressurized condition

The imbibition effects of modified and unmodified BN-LSW composite systems on core samples under pressurized condition were analyzed using NMR T_2 spectra. NMR technology was employed to measure real-time dynamic changes in fluid saturation within the core during imbibition. The resulting NMR T_2 spectra are shown in Figs. 8 and 9.

From Fig. 8, it can be seen that during imbibition under pressurized condition, the T_2 spectrum of the core sample under modified BN-LSW treatment first decreases and then increases. At the initial stage of imbibition, the invasion of modified BN-LSW solution into core pores causes massive oil displacement. The rapid decrease of hydrogen proton concentration leads to significant signal amplitude attenuation. As imbibition continues, the modified BN-LSW solution keeps penetrating into core pores. The

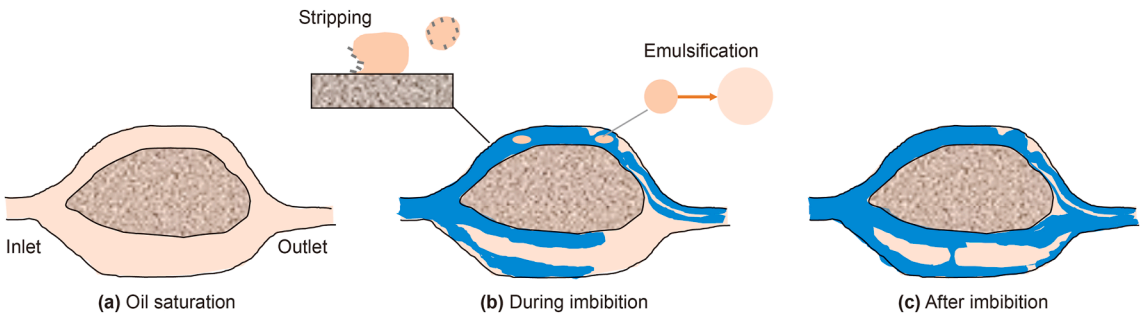

Fig. 6. Ambient-pressure imbibition mechanism diagram of core samples in modified BN-LSW composite system.

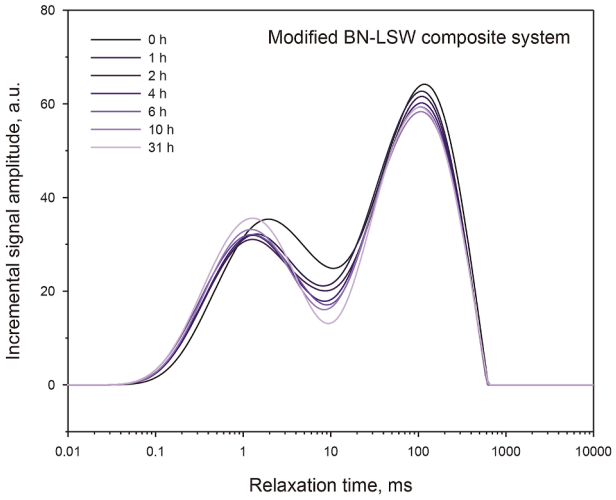

Fig. 8. T_2 spectra of core after imbibition in a modified BN-LSW composite system under pressurized condition.

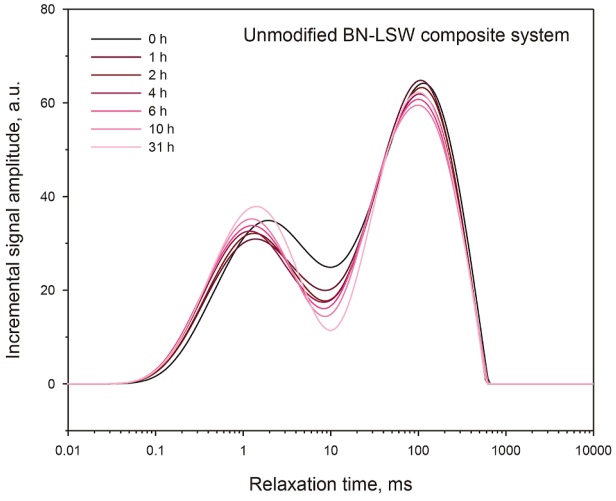

Fig. 9. T_2 spectra of core after imbibition in an unmodified BN-LSW composite system under pressurized condition.

gradual recovery of hydrogen proton concentration in pores results in a certain degree of signal amplitude increase.

Fig. 9 shows that the T_2 spectrum of oil-saturated core samples treated with unmodified BN-LSW also exhibits a decreasing-then-increasing trend. Comparing Figs. 8 and 9 reveals that the signal amplitude variation range of the T_2 spectrum envelope for modified BN-LSW is significantly greater than that of unmodified BN-LSW. This indicates that core samples achieve optimal imbibition performance when treated with modified BN-LSW under pressurized condition.

To quantitatively evaluate the imbibition performance difference between modified and unmodified BN-LSW under pressurized condition, we plotted the T_2 spectrum peak area changes of core samples in both solutions at different time points, as shown in Fig. 10.

Fig. 10 shows that the peak areas of both core samples showed a continuous decreasing trend during pressurized imbibition process. After 6 h of imbibition, the small pore peak areas decreased by 61.34 a.u. (modified BN-LSW) and 61.25 a.u. (unmodified BN-LSW), while the large pore peak areas decreased by 2488.50 a.u.

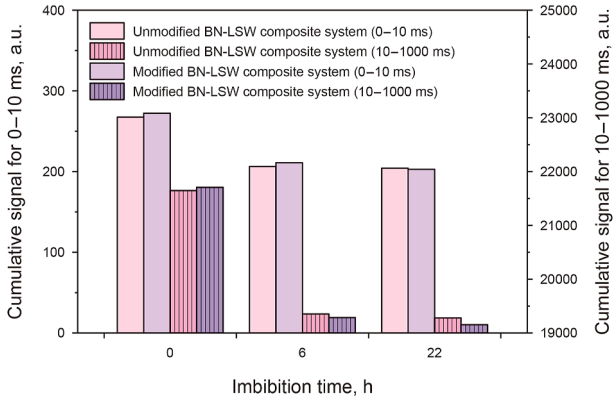

Fig. 10. T_2 peak area evolution during pressurized imbibition in the modified and unmodified BN-LSW composite systems.

(modified BN-LSW) and 2359.70 a.u. (unmodified BN-LSW). After 22 h of imbibition, the small pore peak areas decreased by 69.49 a.u. (modified BN-LSW) and 58.34 a.u. (unmodified BN-LSW), while the large pore peak areas decreased by 2631.30 a.u. (modified BN-LSW) and 2432.70 a.u. (unmodified BN-LSW). The modified BN-LSW composite system exhibited a more significant reduction in peak area under pressurized conditions, indicating its superior ability to displace crude oil from core pores and achieve better imbibition effects.

3.3.3. Imbibition mechanism of modified BN-LSW composite system under pressurized condition

The imbibition mechanism of the modified BN-LSW composite system under pressurized condition was analyzed with NMR T_2 spectrum measurements. Fig. 11 illustrates the imbibition mechanism of oil-saturated core samples under pressurized condition and the action of the modified BN-LSW composite system.

From Fig. 11, it can be observed that under pressure-driven conditions, the modified BN-LSW composite system preferentially entered large pores and displaced the crude oil inside. At this stage, the driving force exceeded capillary pressure. Meanwhile, the modified BN-LSW exhibited significant synergistic effects—not only effectively improving rock wettability but also emulsifying with crude oil in the pores, stripping oil films from rock surfaces. Additionally, it significantly reduced crude oil viscosity, thereby greatly enhancing imbibition recovery in large pores. During the early stage of imbibition under pressurized condition, the composite system preferentially entered large rock pores. As imbibition continues, the system reacted with crude oil in small pores, gradually displacing it.

3.4. Imbibition adaptability of the modified BN-LSW composite system in core samples with different permeabilities

3.4.1. Imbibition performance in core samples with different core permeabilities

Oil-saturated core samples with varying permeabilities were placed in a 0.002 wt% modified BN-LSW composite system. Spontaneous imbibition experiments were conducted under ambient pressure, with real-time recording of core mass changes at each time point. After the experiment, the corresponding recovery efficiency vs. time curves were calculated based on mass changes, as shown in Fig. 12.

Fig. 12 shows that for oil-saturated core samples with different permeabilities, the recovery efficiency increased rapidly in the early stage of imbibition, then gradually slowed down and

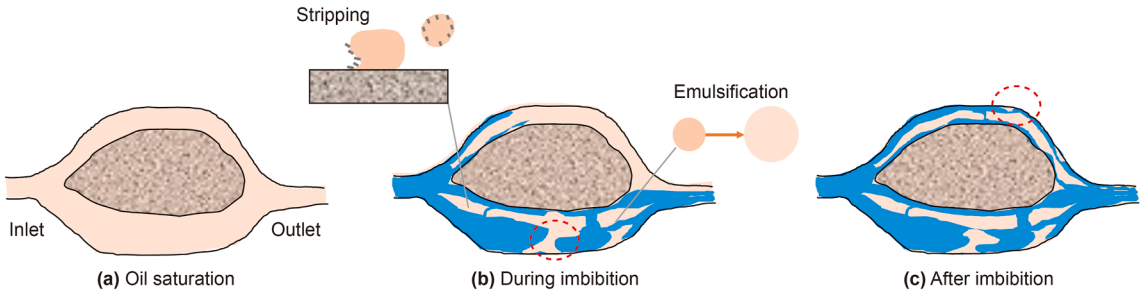

Fig. 11. Pressurized imbibition mechanism diagram of core samples in modified BN-LSW composite system.

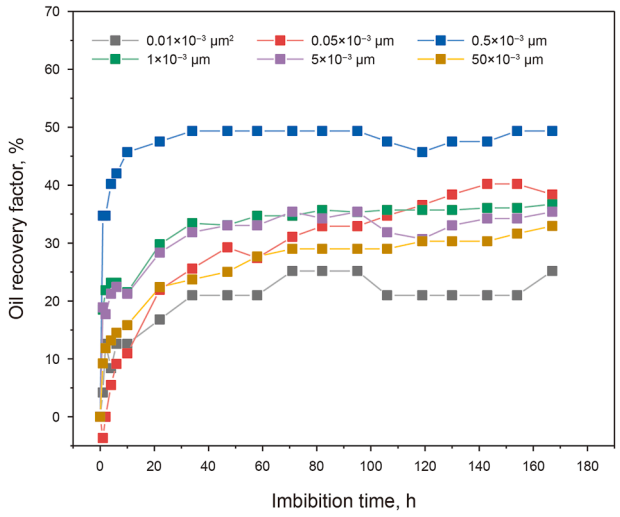

Fig. 12. The imbibition effect of different permeability rock cores in a modified BN-LSW composite system.

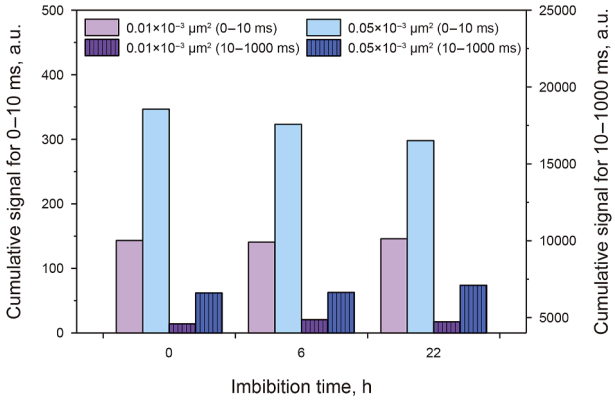

Fig. 13. T_2 spectrum peak area evolution during modified BN-LSW spontaneous imbibition at ambient pressure in core samples with permeabilities of 0.01 × 10^{-3} and 0.05 × 10^{-3} μm².

eventually stabilized. The final recovery efficiency after imbibition first increased and then decreased with rising permeability. The core sample with a permeability of 0.05 × 10^{-3} μm² achieved the highest recovery efficiency of 38.4%, while the sample with 0.01 × 10^{-3} μm² had the lowest recovery efficiency of 25.2%. The modified BN-LSW composite system improved recovery efficiency for core samples of all permeabilities, with the best imbibition effect observed at 0.05 × 10^{-3} μm².

3.4.2. NMR characteristics of the composite system in core samples with different permeabilities

To systematically evaluate the imbibition recovery effects of the modified BN-LSW composite system in core samples of varying permeabilities, a grouped comparative analysis was conducted, dividing the experimental data into three groups for comprehensive assessment.

Core samples with permeabilities of 0.01 × 10^{-3} and 0.05 × 10^{-3} μm² were firstly placed in a 0.002 wt% modified BN-LSW composite system. NMR analysis was performed at different time intervals to obtain T_2 spectrum, and the changes in T_2 spectrum peak area over imbibition time were plotted for both groups, as shown in Fig. 13.

Fig. 13 shows that the small-pore peak area of both core samples first decreases and then increases. After 6 h of imbibition in the modified BN-LSW composite system, the small-pore peak area of the 0.01 × 10^{-3} μm² core decreases by 2.57 a.u., while the large-pore peak area increases by 276.44 a.u. For the 0.05 × 10^{-3} μm² core, the small-pore peak area decreases by 23.47 a.u., and the large-pore peak area increases by 27.12 a.u. This indicates that in the early stage of imbibition, oil displacement in small pores is more significant in higher-permeability cores. After 22 h of imbibition, the small-pore peak area of the 0.01 × 10^{-3} μm² core increases by 2.65 a.u., and the large-pore peak area increases by 138.49 a.u. For the 0.05 × 10^{-3} μm² core, the small-pore peak area decreases by 48.67 a.u., and the large-pore peak area increases by 500.11 a.u. This suggests that the 0.05 × 10^{-3} μm² core has better oil imbibition efficiency in the composite system. The BN-LSW composite system can effectively promote continuous oil production from small pores in low-permeability cores. However, if permeability is too low, nanoparticle aggregation and pore blockage may occur, inhibiting the imbibition process and reducing efficiency.

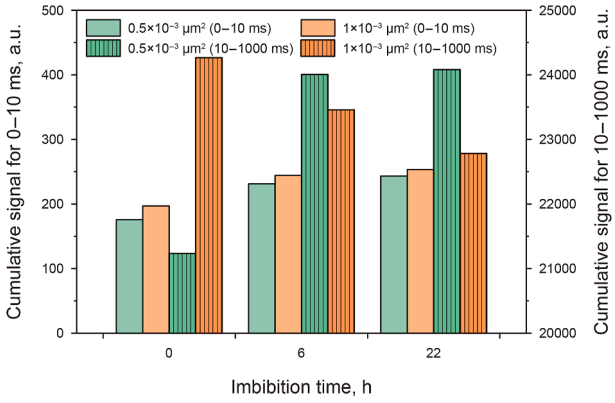

Fig. 14. T_2 spectrum peak area evolution during modified BN-LSW spontaneous imbibition at ambient pressure in core samples with permeabilities of 0.5 × 10^{-3} and 1 × 10^{-3} μm².

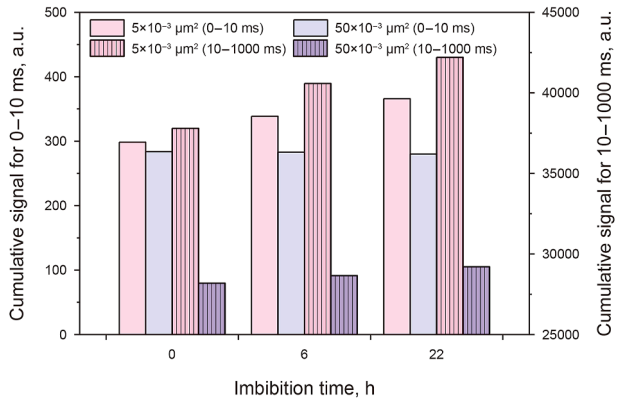

Fig. 15. T_2 spectrum peak area evolution during modified BN-LSW spontaneous imbibition at ambient pressure in core samples with permeabilities of 5×10^{-3} and 50×10^{-3} μm^2.

Core samples with permeabilities of 0.5×10^{-3} and 1×10^{-3} μm^2 were then placed in a 0.002 wt% modified BN-LSW composite system. The changes in T_2 spectrum peak area over imbibition time were plotted for both groups, as shown in Fig. 14.

From Fig. 14, it can be seen that the small pore peak area of both core samples continuously increased with imbibition time. For the 0.5×10^{-3} μm^2 core, the small pore peak area increased by 55.44 a.u. after 6 h of imbibition, while the large pore peak area increased by 2772.20 a.u. In contrast, the 1×10^{-3} μm^2 core showed a 47.18 a.u. increase in small pores but an 806.80 a.u. decrease in large pores. By 22 h, the 0.5×10^{-3} μm^2 core exhibited a further 67.63 a.u. increase in small pores and a continued 2846.70 a.u. increase in large pores. Meanwhile, the 1×10^{-3} μm^2 core had a 56.30 a.u. increase in small pores but a significant 1480.6 a.u. decrease in large pores. Comparing the changes in peak area reveals that the BN-LSW composite system demonstrates superior imbibition performance in the 0.5×10^{-3} μm^2 core.

Core samples with permeabilities of 5×10^{-3} and 50×10^{-3} μm^2 were finally placed in a 0.002 wt% modified BN-LSW composite system. The changes in T_2 spectrum peak area with imbibition time for both core samples in the composite system are plotted in Fig. 15.

From Fig. 15, it can be seen that after 6 h of imbibition, the small pore peak area of the 5×10^{-3} μm^2 core increased by 40.27 a.u., while the large pore peak area increased by 2783.60 a.u. For the 50×10^{-3} μm^2 core, the small pore peak area decreased by 0.78 a.u., and the large pore peak area increased by 463.60 a.u. By 22 h, the 5×10^{-3} μm^2 core showed a 67.48 a.u. increase in small pores and a 4404.40 a.u. increase in large pores. The 50×10^{-3} μm^2 core exhibited a 3.52 a.u. decrease in small pores and a 1019.40 a.u. increase in large pores. These results indicated that the BN-LSW composite system has better imbibition performance in the 5×10^{-3} μm^2 core. However, as permeability further increases, the imbibition effect weakens due to reduced capillary forces.

A comparative analysis of Figs. 13–15 shows that the modified BN-LSW composite system enhances oil recovery efficiency in core samples of different permeabilities. The effect of permeability on the imbibition-recovery performance of the composite system had a critical threshold. The best imbibition effect occurred when the permeability was 0.05×10^{-3} μm^2.

4. Conclusions

Based on previous research of the modified BN-LSW composite system's development and oil displacement experiments, this study tested its imbibition performance in low-permeability cores under both ambient and pressurized conditions using NMR analysis. The following conclusions were drawn:

(1) Compared to the unmodified BN-LSW composite system, the modified BN-LSW composite system exhibited better imbibition-recovery performance under ambient pressure, achieving a final recovery efficiency of 43.92%.
(2) Under ambient-pressure imbibition conditions, the modified BN-LSW composite system mainly used capillary forces. It first entered small pores to push out crude oil, as shown by NMR T_2 signal changes. It effectively improved core wettability and emulsified oil in the pores, enhancing oil recovery from small pores and significantly increasing the recovery degree.
(3) The modified BN-LSW composite system demonstrated superior imbibition performance under pressurized conditions, reaching a final recovery efficiency of 56.52%.
(4) Under pressurized imbibition conditions, the modified BN-LSW system's driving force overcame capillary forces, causing preferential oil displacement in large pores as shown by NMR T_2 signal changes. With continued imbibition, the system then interacted with oil in small pores, gradually drawing oil from these pores too.
(5) The modified BN-LSW system enhanced imbibition recovery in cores with different permeabilities. It performed best at 0.05×10^{-3} μm^2 permeability. When permeability was too high, capillary forces weakened. When permeability was too low, nanoparticles clumped and blocked pores, reducing oil recovery.
(6) NMR technology enabled quantification of the BN-LSW composite system's pore-scale mobilization efficiency during imbibition, thereby elucidating its microscopic oil recovery mechanism across distinct pore sizes.
(7) In this study, the BN-LSW imbibition solution was prepared using NMR-active formation water. The hydrogen nuclei (^{1}H) in water generated background NMR signals that partially interfered with experimental results. Future studies can employ deuterated water (D_2O) to prepare the composite system, eliminating ^{1}H-related signal interference.

CRediT authorship contribution statement

Si Guo: Writing – original draft, Visualization, Validation, Investigation, Data curation. **Jiong Zhang:** Validation, Investigation, Data curation. **Ying-Qi Gao:** Validation, Investigation, Data curation. **Hong-Gen Tan:** Validation, Investigation, Data curation. **Hong-Bin Cheng:** Validation, Investigation, Data curation. **Hong-Yu Li:** Validation, Investigation, Data curation. **Dao-Yi Zhu:** Writing – review & editing, Supervision, Investigation.

Declaration of competing interest

The authors declare that they have no known competing financial interests or personal relationships that could have appeared to influence the work reported in this paper.

References

Al-Asadi, A., Rodil, E., Soto, A., 2022. Nanoparticles in chemical EOR: A review on flooding tests. Nanomaterials 12 (23), 4142. https://doi.org/10.3390/nano12234142.
Arab, D., Kantzas, A., Bryant, S.L., 2018. Nanoparticle stabilized oil in water emulsions: A critical review. J. Petrol. Sci. Eng. 163, 217–242. https://doi.org/10.1016/j.petrol.2017.12.091.

Binks, B.P., Whitby, C.P., 2005. Nanoparticle silica-stabilised oil-in-water emulsions: Improving emulsion stability. Colloids Surf. A Physicochem. Eng. Asp. 253 (1–3), 105–115. https://doi.org/10.1016/j.colsurfa.2004.10.116.

Du, H., 2023. Experimental Mechanism Study on Synergistic Oil Displacement with Multi-effects in Tight Reservoirs. PhD Dissertation. Xi'an Shiyou University. https://doi.org/10.27400/d.cnki.gxasc.2023.001301 (in Chinese).

Eltoum, H., Yang, Y.L., Hou, J.R., 2021. The effect of nanoparticles on reservoir wettability alteration: A critical review. Pet. Sci. 18, 136–153. https://doi.org/10.1007/s12182-020-00496-0.

Feng, Y., Hou, J., Yang, Y., Wang, S., Wang, D., Cheng, T., You, Z., 2022. Morphology of MoS_2 nanosheets and its influence on water/oil interfacial tension: A molecular dynamics study. Fuel 312, 122938. https://doi.org/10.1016/j.fuel.2021.122938.

Kang, W., Jiang, H., Yang, H., Li, Z., Zhou, B., He, Y., Sarenbekuly, B., Gabdullin, M., 2021. Study of nano-SiO_2 reinforced CO_2 foam for anti-gas channeling with a high temperature and high salinity reservoir. J. Ind. Eng. Chem. 97, 506–514. https://doi.org/10.1016/j.jiec.2021.03.007.

Kang, W.L., Zhou, B.B., Issakhov, M., Gabdullin, M., 2022. Advances in enhanced oil recovery technologies for low permeability reservoirs. Pet. Sci. 19 (4), 1622–1640. https://doi.org/10.1016/j.petsci.2022.06.010.

Liang, T., Hou, J., Xi, J., 2023. Mechanisms of nanofluid based modification MoS_2 nanosheet for enhanced oil recovery in terms of interfacial tension, wettability alteration and emulsion stability. J. Dispersion Sci. Technol. 44 (1), 26–37. https://doi.org/10.1080/01932691.2021.1930034.

Liu, S., Liu, X., Zhou, Z., 2019. Simulation method and device for fracturing fluid imbibition to enhance production in dual-porosity dual-permeability reservoir. Chinese Patent: CN110306960B (in Chinese).

Liu, Y.L., Li, Y., Si, Y.F., Fu, J., Dong, H., Sun, S.S., Zhang, F., She, Y.H., Zhang, Z.Q., 2023. Synthesis of nanosilver particles mediated by microbial surfactants and its enhancement of crude oil recovery. Energy 272, 127123. https://doi.org/10.1016/j.energy.2023.127123.

Manshad, A.K., Ali, J.A., Haghighi, O.M., Sajadi, S.M., Keshavarz, A., 2022. Oil recovery aspects of ZnO/SiO_2 nano-clay in carbonate reservoir. Fuel 307, 121927. https://doi.org/10.1016/j.fuel.2021.121927.

Moradi, B., Pourafshary, P., Farahani, F.J., Mohammadi, M., Emadi, M., 2015. Application of SiO_2 nano particles to improve the performance of water alternating gas EOR process. In: SPE Oil and Gas India Conference and Exhibition. https://doi.org/10.2118/178040-MS.

Paryoto, S., Romdoni, Y., Kurnia, I., Muraza, O., Khalil, M., 2023. Synergy of surfactant mixtures and Fe_3O_4 nanoparticles for enhanced oil recovery (EOR). Inorg. Chem. Commun. 155, 111125. https://doi.org/10.1016/j.inoche.2023.111125.

Pereira, M.L., Maia, K.C., Silva, W.C., Leite, A.C., Francisco, A.D., Vasconcelos, T.L., Nascimento, R.S., Grasseschi, D., 2020. Fe_3O_4 nanoparticles as surfactant carriers for enhanced oil recovery and scale prevention. ACS Appl. Nano Mater. 3 (6), 5762–5772. https://doi.org/10.1021/acsanm.0c00939.

Qu, M., Hou, J., Liang, T., Qi, P., 2021. Amphiphilic rhamnolipid molybdenum disulfide nanosheets for oil recovery. ACS Appl. Nano Mater. 4 (3), 2963–2972. https://doi.org/10.1021/acsanm.1c00102.

Qu, M., Liang, T., Hou, J., Liu, Z., Yang, E., Liu, X., 2022. Laboratory study and field application of amphiphilic molybdenum disulfide nanosheets for enhanced oil recovery. J. Petrol. Sci. Eng. 208, 109695. https://doi.org/10.1016/j.petrol.2021.109695.

Raj, I., Qu, M., Xiao, L., Hou, J., Li, Y., Liang, T., Yang, T., Zhao, M., 2019. Ultralow concentration of molybdenum disulfide nanosheets for enhanced oil recovery. Fuel 251, 514–522. https://doi.org/10.1016/j.fuel.2019.04.078.

Shao, W., Yang, J., Wang, H., Chang, J., Wu, H., Hou, J., 2023. Recent research progress on imbibition system of nanoparticle-surfactant dispersions. Capillarity 8 (2), 34–44. https://doi.org/10.46690/capi.2023.08.02.

Tang, W., Zou, C., Liang, H., Da, C., Zhao, Z., 2022. The comparison of interface properties on crude oil-water and rheological behavior of four polymeric nanofluids (nano-SiO_2, nano-CaO, GO and CNT) in carbonates for enhanced oil recovery. J. Petrol. Sci. Eng. 214, 110458. https://doi.org/10.1016/j.petrol.2022.110458.

Wang, W., Peng, Y., Chen, Z., Liu, H., Fan, J., Liu, Y., 2022. Synergistic effects of weak alkaline–surfactant–polymer and SiO_2 nanoparticles flooding on enhanced heavy oil recovery. Energy Fuels 36 (14), 7402–7413. https://doi.org/10.1021/acs.energyfuels.2c01096.

Wu, H., Gou, C., Li, J., Lu, Y., Liu, H., Tan, R., Hou, J., 2024a. Synergistic system of alkyl polyglucoside and amine oxide for enhanced oil recovery. Energy Fuels 38 (7), 5791–5799. https://doi.org/10.1021/acs.energyfuels.4c00434.

Wu, H., Hou, K., Xu, G., Li, G., Chang, J., Luan, T., Shao, W., Hou, J., 2024b. CO_2 switchable Pickering emulsion stabilized by responsive Janus SiO_2 nanoparticles for enhanced oil recovery. ACS Appl. Nano Mater. 7 (2), 1835–1844. https://doi.org/10.1021/acsanm.3c05079.

Wu, H., Luo, Y., Li, G., Yuan, Y., Chang, J., Kang, N., Hou, J., 2025. Enhanced oil recovery using amphiphilic nanomaterials with tailored functionalities: A review. J. Mol. Liq. 425, 127190. https://doi.org/10.1016/j.molliq.2025.127190.

Xiao, L., Hou, J., 2023. Study on the adsorption laws and enhanced oil recovery of nanofluid prepared by amphiphilic nanosheets in the low-permeability porous media. Ind. Eng. Chem. Res. 63 (1), 252–264. https://doi.org/10.1021/acs.iecr.3c03220.

Xiao, L., Hou, J., Qu, M., Wang, W., Wen, Y., Liang, T., Wu, W., Qi, P., 2022. Laboratory study and field application of high temperature resistant and permeable flooding nanofluid for enhanced spontaneous imbibition oil recovery. In: SPE Annual Technical Conference and Exhibition. https://doi.org/10.2118/210005-MS.

Xu, D., Bai, B., Wu, H., Hou, J., Meng, Z., Sun, R., Li, Z., Lu, Y., Kang, W., 2019. Mechanisms of imbibition enhanced oil recovery in low permeability reservoirs: Effect of IFT reduction and wettability alteration. Fuel 244, 110–119. https://doi.org/10.1016/j.fuel.2019.01.118.

Xu, G., Chang, J., Wu, H., Shao, W., Li, G., Hou, J., Kang, N., Yang, J., 2023. Enhanced oil recovery performance of surfactant-enhanced Janus SiO_2 nanofluid for high temperature and salinity reservoir. Colloids Surf. A Physicochem. Eng. Asp. 657, 130545. https://doi.org/10.1016/j.colsurfa.2022.130545.

Yang, C., Yang, E., Dong, C., Che, Y., 2025. A method for enhancing production in tight oil reservoir volume fracturing based on imbibition mechanism. Chinese Patent. CN119825324B. (in Chinese).

Yang, H.B., Jiang, H.Z., Xu, Z., Zhang, X., Wang, T., Liu, H.N., Ma, X., Zhu, J.J., Zhang, X. F., Kang, W.L., 2025. Development and evaluation of organic/metal ion double crosslinking polymer gel for anti-CO_2 gas channeling in high temperature and low permeability reservoirs. Pet. Sci. 22 (2), 724–738. https://doi.org/10.1016/j.petsci.2024.11.016.

Yang, Y., Yuan, W., Hou, J., You, Z., Li, J., Liu, Y., 2020. Stochastic and upscaled analytical modeling of fines migration in porous media induced by low-salinity water injection. Appl. Math. Mech. 41 (3), 491–506. https://doi.org/10.1007/s10483-020-2583-9.

Zhu, D., Qin, J., Gao, Y., Guo, S., Bai, L., Zhao, Y., Zhao, Q., Zhang, H., 2023. Black nanosheet-enhanced low-salinity water system for improving oil recovery in a low-permeability conglomerate reservoir. Energy Fuels 37 (16), 11893–11901. https://doi.org/10.1021/acs.energyfuels.3c02258.

Zhu, D., Gao, Y., Bai, L., Guo, S., 2024a. Development of anionic-modified black nanosheet and its oil imbibition performance in ultralow-permeability reservoirs. Energy Fuels 38 (15), 14149–14157. https://doi.org/10.1021/acs.energyfuels.4c02952.

Zhu, D., Qin, J., Gao, Y., Zhang, J., Guo, S., Liu, S., Zhao, J., Gao, Y., 2024b. Dispersion stability and oil displacement effect of modified black nanosheet. Energy Fuels 38 (13), 11635–11643. https://doi.org/10.1021/acs.energyfuels.4c02155.

Zhu, D., Guo, S., Lu, J., Yang, Y., Zhang, T., Zhang, J., Gao, Y., Tan, H., Cheng, H., Li, H., 2025. Influence of injection parameters of black nanosheets on enhancing oil recovery performance in low-permeability reservoirs. Energy Fuels 39 (13), 6241–6250. https://doi.org/10.1021/acs.energyfuels.5c00546.